

1 **Fluctuation of cellular differentiation in limb regeneration is**  
2 **regulated by Pde4b in urodele amphibians.**

3 Akira Satoh<sup>1,2</sup>, Rena Kashimoto<sup>2</sup>, Ayaka Ohashi<sup>2</sup>, Saya, Furukawa<sup>3</sup>, Sakiya Yamamoto<sup>3</sup>, Takeshi Inoue<sup>4</sup>,  
4 and Toshinori Hayashi<sup>5,6</sup>, Kiyokazu Agata<sup>7</sup>

5

6 Affiliations:

7 1) Okayama University, Research core for interdisciplinary sciences (RCIS), Okayama, Japan

8 2) Okayama University, Graduate School of Environmental and Life Science, Okayama, Japan

9 3) Okayama University, faculty of science, department of biological sciences, Okayama, Japan

10 4) Tottori University, Division of Adaptation Physiology, Faculty of Medicine, Tottori, Japan

11 5) Amphibian Research Center, Hiroshima University, Hiroshima, Japan

12 6) Graduate School of Integrated Sciences for Life, Hiroshima University, Hiroshima, Japan

13 7) Laboratory of Regeneration Biology, National Institute for Basic Biology, Okazaki, Japan

14

15 **Author for Correspondence**

16 Akira Satoh

17 Okayama University

18 Research Core for Interdisciplinary Sciences (RCIS)

19 3-1-1, Tsushima-naka, Kitaku, Okayama, 700-8530, Japan

20 Tel: +81-86-251-8421

21 Email: [satoha@cc.okayama-u.ac.jp](mailto:satoha@cc.okayama-u.ac.jp)

22

23 **Key words:** *Pde4b*, limb regeneration, *Pleurodels waltl*, *Ambystoma mexicanum*, dedifferentiation,  
24 reprogramming

25

26

27

28

29

30 ***Abstract***

31 Urodele amphibians, *Pleurodeles waltl* and *Ambystoma mexicanum*, have organ-level regeneration  
32 capability, such as limb regeneration. Multipotent cells are induced by an endogenous mechanism in  
33 amphibian limb regeneration. It is well known that dermal fibroblasts receive regenerative signals and  
34 turn into multipotent cells, called blastema cells. However, the induction mechanism of the blastema  
35 cells from matured dermal cells was unknown. We previously found that BMP2, FGF2, and FGF8  
36 (B2FF) could play sufficient roles in blastema induction in urodele amphibians. Here, we show that  
37 B2FF treatment can induce dermis-derived cells that can participate in multiple cell lineage in limb  
38 regeneration. We first established a newt dermis-derived cell line and confirmed that B2FF treatment on  
39 the newt cells provided plasticity in cellular differentiation in limb regeneration. Interspecies  
40 comparative analysis clarified that *Pde4b* upregulation by B2FF specifically took place in the newt cells.  
41 Blocking PDE4B signaling by Rolipram suppressed dermis-to-cartilage transformation and the mosaic  
42 knockout animals showed consistent results. Our results are a valuable insight into how dermal  
43 fibroblasts acquire multipotency during the early phase of limb regeneration *via* an endogenous program  
44 in amphibian limb regeneration.

45 Urodele amphibians can regenerate various organs including limbs. In their appendage  
46 regeneration, a structure called a blastema is induced after organ damage, and the induction of blastema  
47 is responsible for successful appendage regeneration. In other words, no blastema formation essentially  
48 results in no appendage regeneration. Thus, understandings of blastema formation would be the closest  
49 way to elucidate the ability of organ-level regeneration in urodele amphibians. And limb regeneration is  
50 an ideal model to study blastema formation and the organ-level regeneration ability in urodele  
51 amphibians.

52 Limb regeneration necessarily accompanies blastema formation, which has been considered to  
53 be a similar structure to a developing limb bud<sup>1</sup>. A regeneration blastema actually showed a similar gene  
54 profile to a developing limb bud<sup>2</sup>. Thus, a mechanism to induce a re-developmental field in an adult  
55 body has been investigated with great curiosity. From this angle, two issues are embossed: 1) how is the  
56 re-developmental field induced? 2) how do the differentiated cells turn into cells with an embryonic gene  
57 profile? Regarding blastema induction, classic studies clearly demonstrated that the nerves play a central  
58 role in the process<sup>3,4</sup>. Denervation from limbs results in no regeneration after limb amputation. Wound  
59 healing takes place instead. The amputation plane is covered by the migrating epidermis immediately  
60 after limb amputation. After the epidermal covering of the exposed amputation surface, the nerves secrete  
61 some factors to create a regenerative environment. Molecules, which are secreted from the nerve ends  
62 and contribute to creating the regenerative environment in an amputated limb, had been investigated for  
63 a long time. Some factors have been identified as nerve factors<sup>5,6,7</sup>. Among them, FGFs and BMPs can  
64 induce a blastema in multiple species and organs<sup>8</sup>. *Fgf2*, *Fgf8*, and *Bmp2* are expressed axolotl neurons  
65 in the dorsal root ganglion (DRG). Application of FGF2+FGF8+BMP2 (B2FF) to the wounded skin  
66 results in blastema formation instead of skin wound healing in urodeles<sup>8</sup>. FGF2+FGF8 without BMP2  
67 (FF) can induce a blastema. However, the FF-induced blastema does not have the ability to keep  
68 growing up to a patterned limb. BMP2 induced structure lacks proper blastema gene expressions and  
69 does not have the ability to grow a limb<sup>8</sup>. Downregulation of those genes in DRG neurons resulted in  
70 decreasing in the limb regeneration ability<sup>9</sup>. Thus, FGF2, FGF8, and BMP2 can work as nerve-secreting  
71 molecules and regeneration inducers in urodele amphibians. Thanks to the determination of the inductive  
72 molecules, an approach to the other issue of how the differentiated cells turn into an embryonic state can  
73 be possible.

74 A regeneration blastema fulfilled by undifferentiated cells is induced on the amputation plane,  
75 below which differentiated tissues exist. Undifferentiated blastema cells, having an embryonic profile,  
76 emerged from the differentiated tissues<sup>2</sup>. The dermis is the major source of blastema cells among the  
77 limb tissues<sup>10,11</sup>. Dermal fibroblasts have been considered to turn into blastema cells. Dermis-derived

78 blastema cells can change their cell type into varied connective tissue lineage, such as cartilage. Such  
79 transdifferentiation ability is restricted within the connective tissue lineage<sup>10, 12, 13</sup>. This is consistent that  
80 a blastema has a similar gene expression profile to a developing limb bud. Limb bud cells derived from  
81 the lateral plate mesoderm can participate in varied connective tissue lineages, but not other  
82 non-connective tissues, such as the muscle<sup>14</sup>. Considering these, dermal fibroblasts may get  
83 reprogrammed and become limb bud-like cells. On the other hand, another possibility can explain the  
84 emergence of blastema cells from the differentiated dermis. It is well known that multipotent stem cells  
85 exist throughout the body. The dermis involves many cells. Thus, it is feasible that the axolotl dermis  
86 contains stem cells, and that the stem cells participate in blastema formation. However, molecular and  
87 histological descriptions are largely unknown.

88         The determination of the regeneration induction molecules makes us possible to investigate  
89 molecular regulations, which dermis-derived cells receive just after limb amputation. Most blastema  
90 cells are derived from the dermis<sup>10</sup>. And the dermis-derived cells show connective tissues-restricted  
91 multipotency in limb regeneration<sup>10, 12, 13</sup>. The multipotent blastema cells can be induced by B2FF  
92 application in axolotls. Hence, investigation of a regulation downstream of B2FF in dermal fibroblasts  
93 leads to understandings of cellular reprogramming in amphibian organ regeneration.

94         Here, we explored the downstream gene network of B2FF by comparing gene expressions *in*  
95 *vitro*. We used mouse dermal fibroblasts as a representative of non-regenerative animals and newt skin  
96 fibroblasts as a representative of regenerative animals for the comparative analysis. The following *in*  
97 *vivo* experiments were performed using axolotls because of the benefits of fluorescent observation. The  
98 function of *Pde4b* in conferring multipotency was investigated by the usage of a chemical compound  
99 and the mosaic *Pde4b* crispants. Our findings provide important insights into the generation of  
100 multipotent cells during limb regeneration in caudate amphibians.

101

102

103 **Results**

104 We first developed an *in vitro* system to investigate the blastemal transformation of dermal  
105 fibroblasts. We cannot keep axolotl cells in the satisfyingly proliferative state for a long time. Cultured  
106 axolotl cells were inevitable that they decrease in cell division and undergo senescence state after a  
107 couple of passages. Dermal fibroblasts derived from newts, however, were highly mitotic and could be  
108 stably cultured for a long time. Newt cell line was established from an animal that stably expresses red  
109 fluorescent proteins on the cell membrane (Fig. 1A, B, E, F). Due to the property of the  
110 membrane-anchored mCherry, the fluorescent signal was observed on the cell membrane and shows the  
111 spotted pattern (Fig. 1E, F). The growth rate was approximately 1 doubling per week (Fig. 1G). To  
112 investigate the blastemal transformation of the cells, we treated the cultured cells with the regeneration  
113 inductive molecules (B2FF: Fig. 1C, D). No significant change was observed after 48 hours by B2FF  
114 treatment. However, B2FF treated cells showed large cell aggregates 2 weeks after the treatment (Fig.  
115 1H2, J). No cellular aggregates were observed in the control (Fig. 1H1, I). Sections of the cell aggregates  
116 were prepared and gene expression of blastemal marker genes was investigated by *in situ* hybridization.  
117 *Msx1* expression was confirmable throughout the cell aggregates (Fig. 1K), and *Msx2* expression was  
118 much intense in the surface area (Fig. 1L). The signal of *Prrx1* and *Pea3* were weak but recognizable  
119 (Fig. 1M, N) as compared to the control (Fig. 1O). These results suggest that newt skin fibroblasts can  
120 react with B2FF under *in vitro* environment.

121 We transplanted the cell aggregates into an axolotl blastema to investigate the differentiation  
122 capability of cells involved in the aggregate. Xenografting of newt cells into axolotl tissues had been  
123 described previously<sup>15</sup>. Newt cells can survive in axolotl tissues for a month. Because of the  
124 transparency of an axolotl limb as compared to a newt limb, axolotl limbs are much useful to trace  
125 grafted cells in limb regeneration. The B2FF induced aggregate could be easily removed from the plastic  
126 dish and transplanted into an axolotl mid-bud blastema (Fig. 2A). Regarding the control (non-treated),  
127 the cultured cells never form aggregates. Hence, cell sheets were collected using a scraper and  
128 transplanted into an axolotl blastema (Fig. 2A). Axolotl limbs are relatively transparent, which allows the  
129 trace of the grafted cells by the red-fluorescent (Fig. 2B, C). The grafted newt fibroblasts could survive  
130 in the axolotl tissues and participate in a regenerate (Fig. 2B, C). To explore cellular contribution,  
131 regenerated limbs were sectioned (Fig. 2D–F). Immunofluorescent analysis revealed the location of the  
132 grafted cells (red) and cartilage formation (Col2a; green) in the regenerate (Fig. 2D–F). Little mCherry<sup>+</sup>  
133 was found in the cartilage when the control cells (non-treated) were transplanted (Fig. 2D1-3). In  
134 contrast, the mCherry<sup>+</sup> cells were identifiable within the cartilage region when the B2FF treated cells  
135 were grafted (Fig. 2E1-3). The mCherry signals were always weakened in the cartilage due to the

136 cartilage properties. Cell surface-located and spotted red signals were observable, consisting of the  
137 fluorescent pattern observed in Fig. 1F (Fig. 2F). Furthermore, it was suggested that dermis-derived cells  
138 can redifferentiate into various connective cell types<sup>10, 12, 13</sup>. To clarify whether mCherry<sup>+</sup> cells were  
139 observed in other connective tissues, we focused on the tendons. Tenascin is a marker of tendons and  
140 ligaments and is expressed in the connecting region between skeletal structures and muscles in  
141 amphibians<sup>16</sup>. Tenascin expression was visualized by immunofluorescence (Sup. Fig.1). Tenascin  
142 expression was observed in the peripheral region of the epiphysis and some fibroblast near the epiphysis  
143 (Sup. Fig.1A). Confocal observation confirmed that tenascin was located by the mCherry<sup>+</sup> cells,  
144 suggesting that the mCherry<sup>+</sup> cell became the tendon cell (Sup. Fig.1B, C). Those data suggest that the  
145 grafted B2FF treated newt fibroblasts participated in some connective tissue lineage.

146 Next, the comparative RNA-Seq analysis was conducted in order to identify the genes related  
147 to the acquisition of multipotency. To investigate gene dynamics prior to the formation of cell aggregate,  
148 cells 48 hours after B2FF treatment were harvested for comparison. Furthermore, to focus on the specific  
149 gene dynamics in the regeneration-competent animals, mouse cells were used as a comparison. Mouse  
150 dermal fibroblasts were collected from neonates and 5 passages were undergone before the experiment.  
151 B2FF treatment was performed for 48 hours. RNA-seq was performed by CAGE-seq. To compare gene  
152 expression between newts and mice, gene symbols were used in this comparison. This was because of  
153 the lack of fixed genome information of *Pleurodeles waltl*. Thus, a precise orthologue determination  
154 could not be fixed. We found 4185 genes were commonly expressed in the cultured cells of both species  
155 (Fig. 3A, Supplemental Data 1). Apparently, no huge different profiles could be found as both species  
156 were compared (Fig. 3A). B2FF treatment did not change the gene profile greatly as shown in Fig. 3A.  
157 Among those genes, we selected the genes showing  $FC < -0.5$  and  $FC > 0.6$ . We found that there were 42  
158 genes affected by B2FF treatment (Fig. 3B, Supplemental Data 1). We found out that *Col1A2*, which is a  
159 major component of the dermis, was down-regulated by B2FF treatment in both species (Supplemental  
160 Data 1). This is consistent with the report, in which an axolotl limb blastema is a less collagenous  
161 structure<sup>17</sup>. We further focused on the genes which react oppositely to B2FF in the two species (Fig. 3B).  
162 *Fblim*, *Loxl2*, *Pde4b*, *Spry1*, *Timp3* were upregulated in newt cells and down-regulated in mouse cells by  
163 B2FF treatment. *Adra2a* showed opposite dynamics. To confirm the RNA-seq results, quantitative  
164 RT-PCR (qPCR) analysis was performed (Fig. 3C). The gene expression profiles were consistent with  
165 the results from RNA-seq. (Fig. 3C).

166 These 6 genes dynamics were also investigated in axolotl blastemas (Fig. 4). As mentioned,  
167 axolotls have many advantages *in vivo* experiments. Thus, we investigated the gene expression patterns  
168 in axolotl blastemas in order to perform further experiments in axolotls. qPCR analysis revealed that

169 *Fblim*, *Loxl2*, *Pde4b*, *Spry1*, *Timp3* were upregulated in the blastema. *Fblim1*, *Loxl2*, and *Pde4b* showed  
170 quick upregulation after limb amputation (Fig. 4). Only *Pde4* expression was settled down at 10 days  
171 post-amputation (dpa). *Spry1* and *Timp3* have a late-activation profile in axolotl limb blastemas. *Adra2a*  
172 expression was not detectable throughout the period we tested. These gene expression patterns were  
173 confirmed by *in situ* hybridization. (Fig. 5). Consistently, *Adra2a* was not detectable at 2, 5, and 10 dpa  
174 (Fig. 5A, A', G, G', M, M'). *Fblim1* expression could be recognized in the amputation region from 2 dpa  
175 to 10 dpa (Fig. 5B, H, N). The signal of *Fblim1* could be observed at the border of the amputation plane  
176 (Fig. 5B'), but the signal was weakened in the later time points in the stump regions (Fig. 5H', N').  
177 *Loxl2* expression could also be detected from 2 dpa (Fig. 5C, I, O). The *Loxl2* expression was confirmed  
178 in the part of the basal layer of the blastema epithelium (Fig. 5C, I). *Loxl2* activation was relatively  
179 specific in the distal (blastemal) region and not apparent in the stump region (Fig. 5C', I', O').  
180 Upregulation of *Loxl2* likely takes place in the specific cells, rather broader blastema mesenchymal cells.  
181 *Pde4b* was upregulated in the early stages (2 and 5 dpa; Fig. 5D, J). The upregulation of *Pde4b* could  
182 also be observed around the amputation sites 2 and 5 dpa (Fig. 5D', J'). But *Pde4b* expression was  
183 down-regulated in the later stages (10 dpa) (Fig. 5P, P'). *Spry1* signals were not obvious 2 dpa in both  
184 the distal and the proximal region (Fig. 5E, E'). But the signal became confirmable in the blastema 5 and  
185 10 dpa in the blastema (Fig. 5K, Q). *Spry1* expression was also observed around the amputation site 5  
186 dpa (Fig. 5K'). No signal was confirmed in the stump region 10 dpa (Fig. 5Q') Upregulation of *Timp3*  
187 could be detected 2 and 5 dpa (Fig. 5F, L). However, the *Timp3* signal was weakened in the proximal  
188 region of the blastema although the distal blastema maintains a relatively high level of *Timp3* expression  
189 at 10 dpa (Fig. 5R). The faint signal could also be observed around the amputation site 2 dpa (Fig. 5F').  
190 But no signal could be detected in the proximal region 5 and 10 dpa (Fig. 5L', R') Those data suggest  
191 that the selected 5 genes from the RNA-seq in mouse and newt cells were consistently upregulated in the  
192 axolotl blastema.

193           Instability of cellular differentiation should be induced in the early phases prior to blastema  
194 formation. Blastemas at 5 dpa have been reported to express blastema marker genes and blastemas at the  
195 time point sometimes take a dome shape containing blastema cells<sup>18</sup>. Moreover, the induction  
196 mechanism of cellular dedifferentiation and maintenance mechanism of an undifferentiated state would  
197 be different. Considering those, genes related to the induction of instability of cellular differentiation  
198 would be upregulated in early, and down-regulated in later. From this point of view, we thought *Pde4b*,  
199 which showed early upregulation and late down-regulation, was suitable for this criteria.

200           We next attempted to inhibit *Pde4b* functions in limb regeneration using a chemical inhibitor,  
201 Rolipram. Rolipram binds to the catalytic sites of PDE4B at several amino acids, where are 100%

202 conserved between human PDE4B and axolotl PDE4B (Sup. Fig. 2). It is well known that PDE4B has a  
203 function to hydrolyze cAMP to 5'AMP<sup>19</sup>. To confirm the inhibitory effects to PDE4B in axolotl tissues,  
204 cAMP concentration in axolotl limbs was measured by ELISA (Fig. 6A). Consistently, cAMP  
205 concentration in limb tissues was upregulated by the 7 day-Rolipram treatment (Fig. 6A). This suggests  
206 that Rolipram can effectively inhibit hydrolysis of cAMP by PDE4B in axolotl limbs. Next, we  
207 investigated the dermal fibroblast's transdifferentiation into cartilaginous cells in the presence of  
208 Rolipram (Fig. 6B–E). The limb skin from a GFP animal was transgrafted onto a normal animal, and the  
209 grafted limb was kept a week for the recovery from the grafting damages (Fig. 6B). Then, the limb was  
210 amputated, and the limb-amputated animals were kept in Rolipram-containing water until digits were  
211 identifiable (Fig. 6B, C1-C3). The GFP positive domain was expanded from the amputation stump to the  
212 digit tips of the regenerate (Fig. 6C1-3). The regenerates were fixed and sectioned. *Col2A1*<sup>+</sup> cartilage  
213 cells were revealed by *in situ* hybridization and the location of the GFP<sup>+</sup> cells was revealed by  
214 immunofluorescence (Fig. 6D, E). In the control samples, GFP<sup>+</sup> cells were observable in the *Col2A1*<sup>+</sup>  
215 region (Fig. 6D, Table 1). Five limbs were obtained and sectioned. Sectioning was performed on the  
216 entire limb along the dorsoventral axis. Only sections with GFP<sup>+</sup> cells in the mesenchymal region on the  
217 prepared sections were extracted, and the GFP<sup>+</sup> cells were counted. We found 3321 GFP positive cells in  
218 104 extracted sections, of which 149 GFP positive cells were *Col2A1*<sup>+</sup>. In the Rolipram-treated animals,  
219 GFP<sup>+</sup> cells were little observed in the *Col2A1*<sup>+</sup> region (Fig. 6E, Table 1). We obtained 36 sections from 7  
220 Rolipram-treated samples. Although the number of sections obtained from a single limb sample was  
221 about the same as the control, the number of sections to be extracted in the Rolipram-treated samples  
222 was lower as compared to the control. This was because of the poor participation of GFP<sup>+</sup> cells in the  
223 regenerates compared to controls. Using the same method of cell counting as the control, we observed  
224 only one *Col2A1*<sup>+</sup> cell out of 462 GFP<sup>+</sup> cells (Table 1). It is also noteworthy that cartilage formation in  
225 regenerates was not influenced by the Rolipram treatment. These suggest that Rolipram treatment  
226 increases cAMP concentration in tissues resulting in suppression of the transdifferentiation from dermal  
227 fibroblasts to cartilaginous cells.

228 We further investigated increasing in cAMP concentration impaired cartilage  
229 transdifferentiation from dermal fibroblasts. Dibutyryl-cAMP is a cell-permeable cAMP analog that  
230 activates cAMP-dependent protein kinases<sup>20</sup>. Similarly, GFP<sup>+</sup> skin was transgrafted onto a normal  
231 animal and the GFP skin-grafted limb was amputated to trace the lineage of GFP<sup>+</sup> cells in the absence or  
232 presence of dibutyryl-cAMP (Fig. 7A). The amputated limbs were kept until the regenerates reached the  
233 digit stage (Fig. 7B, F). To visualize GFP and Col2A1, we performed immunofluorescence on the  
234 identical sections (Fig. 7C–I). In the control sample, GFP<sup>+</sup> cells in the cartilaginous region could be



235 detected as well as epidermis and dermis (Fig. 7C–E). On the other hand, the Dibutyl-cAMP treated  
236 limbs showed a little number of GFP<sup>+</sup> cells in the cartilaginous region (Fig. 7G–I). We plotted the rate of  
237 the GFP<sup>+</sup>/Col2A1<sup>+</sup> in the regenerates (Fig. 7J). We counted 13 sections from 8 independent animals in  
238 the control and 21 sections from 17 independent animals in the Dibutyl cAMP-treated animals. It is  
239 noteworthy that the two exceptional plots in the Dibutyl cAMP-treated samples were derived from an  
240 identical animal. These results consistently suggest that cAMP concentration influences a fluctuation of  
241 differentiation of dermal fibroblasts.

242 Next, we attempted to inhibit PDE4B in cultured newt cells by Rolipram (Fig.8). The newt  
243 cells were cultured as above. The control (no B2FF) and the B2FF treated cells gave rise to the sheet and  
244 the aggregate formation, respectively (Fig. 8B–D). Rolipram application into B2FF culture media  
245 resulted in no aggregate formation (Fig. 8E; n=6/6). We grafted the <sup>+</sup>Rolipram/<sup>+</sup>B2FF cell as a sheet  
246 since no aggregate formation could be obtained (Fig. 8A). The participation of the newt cells into  
247 cartilage was assessed at the digit stage. The grafted cells could survive and expand in the regenerate  
248 (Fig. 8F, G). The section revealed that a large number of mCherry<sup>+</sup> newt cells could be observed outside  
249 of the cartilages (Fig. 8H, I). Even though the mCherry<sup>+</sup> newt cells were located just by the regenerated  
250 cartilage, no participation of the grafted newt cells in the cartilage could be observed (Fig. 8J). All cell  
251 counts were shown in Table 2 and Fig. 8K. These results strongly suggest that Rolipram treatment  
252 inhibits re-differentiation from dermal fibroblasts to cartilaginous cells.

253 We next directly manipulated the *Pde4b* gene in axolotls. CRISPR/Cas9 systems allowed to  
254 generate mosaic *Pde4b* knockout animals (*Pde4b* crispants). We had not succeeded in generating  
255 homogenous *Pde4b* crispants. Five crispants were used and the knockout rate was assumed by  
256 ICE-analysis (30-58%, Fig. 9G). We labeled the dermal fibroblasts by GFP electroporation and traced  
257 the lineage during limb regeneration (Fig. 9A–E). The electroporation was performed prior to limb  
258 amputation. The electroporated limb was amputated 3 days after the electroporation, and the animals  
259 were kept until digits were apparent (Fig. 9A, D). In both the control limbs (n=4) and the *Pde4b* crispant  
260 limbs (n=8), GFP<sup>+</sup> cells could be seen in the regenerated limbs (Fig. 9A, B, D, E). The section revealed  
261 that GFP<sup>+</sup> cells could be seen in the *Col2a1*<sup>+</sup> cartilage region and other connective tissues in the  
262 regenerated autopodial region in both the control animals and crispants (Fig. 9C, F). We counted GFP<sup>+</sup>  
263 cells in the regenerated autopodial region (Fig. 9G). Longitudinal sections were made throughout the  
264 regenerate. The GFP<sup>+</sup> and the GFP<sup>+</sup>*Col2a1*<sup>+</sup> cells were counted on all sections. The control limbs, in  
265 which the knockout score was 0, showed that many GFP<sup>+</sup> cells differentiated into *Col2a1*<sup>+</sup> cartilaginous  
266 cells. On the other hand, *Pde4b* crispants showed that much fewer GFP<sup>+</sup> cells participated into *Col2a1*<sup>+</sup>  
267 cartilage. The alignment of the GFP<sup>+</sup>*Col2a1*<sup>+</sup>/GFP<sup>+</sup> ratio with the knockout score calculated from ICE

268 analysis revealed a strong correlation ( $R^2=0.912$ ). Limbs from an animal having a higher knockout score  
269 showed a low integration rate of GFP<sup>+</sup> into a cartilaginous region. In contrast, limbs with a lower  
270 knockout score showed a relatively higher integration rate. This suggests that the *Pde4b* function relates  
271 to the conversion from dermal fibroblasts to cartilage cells in axolotl limb regeneration.  
272  
273

## 274 **Discussions**

### 275 ***The cultured newt cells derived from the dermis***

276 We cultured fibroblasts from a newts' limb skin (dermis), in which many types of cells exist. It  
277 is reasonably assumed that dermal fibroblasts are not homogenous, rather heterogeneous. Moreover, the  
278 determination of fibroblasts is still ambiguous. Thus, it is still difficult to determine the cultured cells we  
279 used precisely. In the present study, we obtained the constantly dividing fibroblasts (Fig. 1). During the  
280 process of establishing the cell line, it is very likely that certain cell populations were selected and  
281 survived. The RNA-Seq data revealed that the cultured fibroblasts express *Coll1a2*, *Vimentin*, and *Twist1*  
282 (Supplemental data 1), which are well-known marker genes as fibroblast marker genes. The expression  
283 profile reasonably suggests dermal fibroblasts were dominantly cultured in our experiment. However,  
284 culturing cells are dividing. Differentiated dermal fibroblasts *in vivo* are assumedly not actively dividing.  
285 Thus, our procedures in cell preparation might somehow transform cells. On the other hand, the cultured  
286 newt cells derived from the dermis did not show cartilage differentiation when the cells were grafted in  
287 the axolotl blastema (Fig. 2). This suggests that the cultured cells were not multipotent and that the  
288 culture condition did not provide multipotency. Further characterization of the cultured cells should be  
289 necessary to determine for precisely describing the cells we used.

290

### 291 ***The xenografting between axolotls and newts***

292 The grafted newts cell could survive and differentiated into a couple of cell types in the axolotl  
293 limb (Fig. 2). Such xenografting between an axolotl and a newt could be found in the histology of the  
294 amphibian regeneration study<sup>21,22</sup>. The grafted tissues and cells functioned physiologically in the  
295 xenografted environments. However, it is still unknown that cells from one species precisely behave  
296 normally in the other. On the other hand, limb regeneration can be induced by B2FF in both species<sup>8</sup>.  
297 B2FF, which we used in order to induce regeneration responses in urodele amphibians, are the  
298 recombinant proteins, whose amino acid sequences are derived from a mouse or a human. Of course, the  
299 axolotl B2FF genes can induce limb regeneration reactions when axolotl B2FF are electroporated<sup>23</sup>.  
300 Thus, mouse B2FF has been considered to activate the same or quite similar gene cascades in both  
301 species. Even though the initial activation mechanism is identical, it is not known that the following  
302 mechanisms are identical or similar. For instance, the time to progress the regeneration stages is different,  
303 implying that the grafted newt cells receive inputs from outside at different timing in an axolotl blastema.  
304 We are not sure how the differences influence the grafted newt cells and their differentiation.

305 The reason why we had to use xenografting in the present study is that we cannot find any  
306 good way to culture axolotl cells for a long time. There are ways to culture the axolotl cells<sup>24,25</sup>.

307 However, it is still tough to have cells that can keep a proliferative state for a long time. To investigate a  
308 more focused and detailed mechanism of dermal fibroblasts' dedifferentiation, finding a way to culture  
309 axolotl cells for a long time is needed.

310

### 311 ***Gene selection***

312 In this paper, we used a unique method for gene selection. We compared mouse fibroblasts  
313 with newt fibroblasts using cultured cells. The comparison would be controversial because mouse cells  
314 and newt cells are physiologically different. While acknowledging the differences in various  
315 physiological properties, we were able to find out candidate genes by comparing the downstream factors  
316 regulated by a common factor, B2FF. In this gene selection, we focused on genes that are inversely  
317 regulated by B2FF treatment in mouse and newt cells. This is based on the finding that the dynamics of  
318 dermal fibroblasts in the axolotl (limb) and mouse (fingertip) regeneration are different<sup>26</sup>. Urodeles can  
319 induce multipotent cells from the dermis, while mice cannot induce multipotent cells from the dermis.  
320 Therefore, we thought that there might be differences in gene expression during the generation of  
321 multipotent cells in the early stages of regeneration. However, it is possible that other systems, such as  
322 epigenetic regulation, are involved in the process of generating pluripotent cells from the dermis, and  
323 further research is needed to determine whether this is reflected in simple differences in transcriptome  
324 expression. Although a multidimensional study is definitely necessary, the fact that we were able to find  
325 a functional molecule in the comparative analysis between the two species in this study provides a  
326 certain amount of positive endorsement for the gene selection method used in this study.

327

### 328 ***Pde4b function in transformation of dermal fibroblasts***

329 We found the *Pde4b* gene from our gene selection. *Pde4b* was upregulated in the very early phase in  
330 axolotl limb regeneration (Fig. 4, Fig. 5D, J). *Pde4b* was downregulated after blastema cell emergence  
331 (Fig. 5P). This expression pattern is reasonable that *Pde4b* has a function in the dedifferentiation stage.  
332 Generally, limb regeneration and development share the same or similar gene cascades to form a  
333 patterned limb after blastema formation. Considering this, the cellular dedifferentiation process is unique  
334 and takes place before blastema formation. Moreover, the functions of cellular dedifferentiation should  
335 be down-regulated after blastema formation because blastema cells are going to be re-differentiated.  
336 Thus, the *Pde4b* gene expression pattern would be suitable as a factor involved in cellular  
337 dedifferentiation.

338 *Pde4b* encodes an enzyme to hydrolyze cAMP to 5'AMP. Thus, PDE4B functions in cAMP  
339 regulation in limb regeneration. It is well known that there are cAMP-dependent pathways, such as the

340 PKA-pathway<sup>27</sup>. Thus, disturbing PDE4B leads to influencing many intracellular signaling cascades.  
341 Downregulation of cAMP in the very early phase of limb regeneration is likely important to  
342 fluctuate cellular differentiation in dermal fibroblasts. This is consistent with the previous report, in  
343 which a low level of cAMP in limb blastemas within 7 days after amputation was described<sup>28, 29</sup>.  
344 Functions of the low level of cAMP at the beginning of limb regeneration have not been investigated.  
345 Our results suggest that a low level of cAMP contributes to fluctuating cellular differentiation in limb  
346 regeneration. On the other hand, cAMP-dependent activities are unlikely to have severe influences on  
347 limb regeneration. PDE4B inhibition by Rolipram resulted in increasing in cAMP concentration in  
348 tissues and impairing the rate of transdifferentiation from dermal fibroblasts to cartilaginous cells.  
349 However, no skeletal pattern defects were observed. Previous reports strongly suggest that organ-level  
350 regeneration can be achieved by lineage-restricted cells, with no transdifferentiation<sup>13</sup>. Considering this,  
351 it is reasonable that a fluctuation of cellular differentiation has little influence on the outcome of limb  
352 regeneration. Although the fluctuation of cellular differentiation does have little influence on limb  
353 regeneration, the mechanism of induction of multipotent cells from differentiated tissues has been  
354 valuable. Blastema cells raised from dermal fibroblasts have been considered to be similar to limb bud  
355 cells. The connective tissue lineage-restricted multipotency is just like that of lateral plate mesoderm  
356 derived limb bud cells. Thus, a mechanism of acquisition of multipotency in dermal fibroblasts might be  
357 closely related to the reactivation of developmental programs. We believe that reprogramming of cellular  
358 differentiation and/or rewinding developmental programs can be learned from amphibian organ  
359 regeneration.  
360

361 **Table 1:** The cell count of GFP<sup>+</sup> Col2a1<sup>+</sup> cells in Rolipram treated limbs

	Number of specimens	Number of pictures	Count for GFP+ Cells	Count for GFP+/Col2A1+	Ratio(%)
CTRL(DMSO)	5	104	3321	149	4.49
Rolipram	7	36	462	1	0.22

362

363

364 **Table 2:** The cell count of Col2a1<sup>+</sup> mCherry<sup>+</sup> cells in newt-cell grafted axolotl limbs

	Number of specimens	number of pictures	Count for mCherry+ cels	Count for Col2A+/mCherry+ cells	Ratio (%)
CTRL	7	19	525	8	1.5
+B2FF	4	13	799	256	32.0
+B2FF/+Rolipram	4	10	331	7	2.1

368

369 ***Acknowledgements***

370 We are grateful Ms. R. Hori for taking a role in cell counting and Ms T. Satoh for general  
371 support for conducting the experiments. This work was supported by AMED (18bm0704006h0003) and  
372 JSPS Grant-in-Aid for Scientific Research (B) (20H03264).

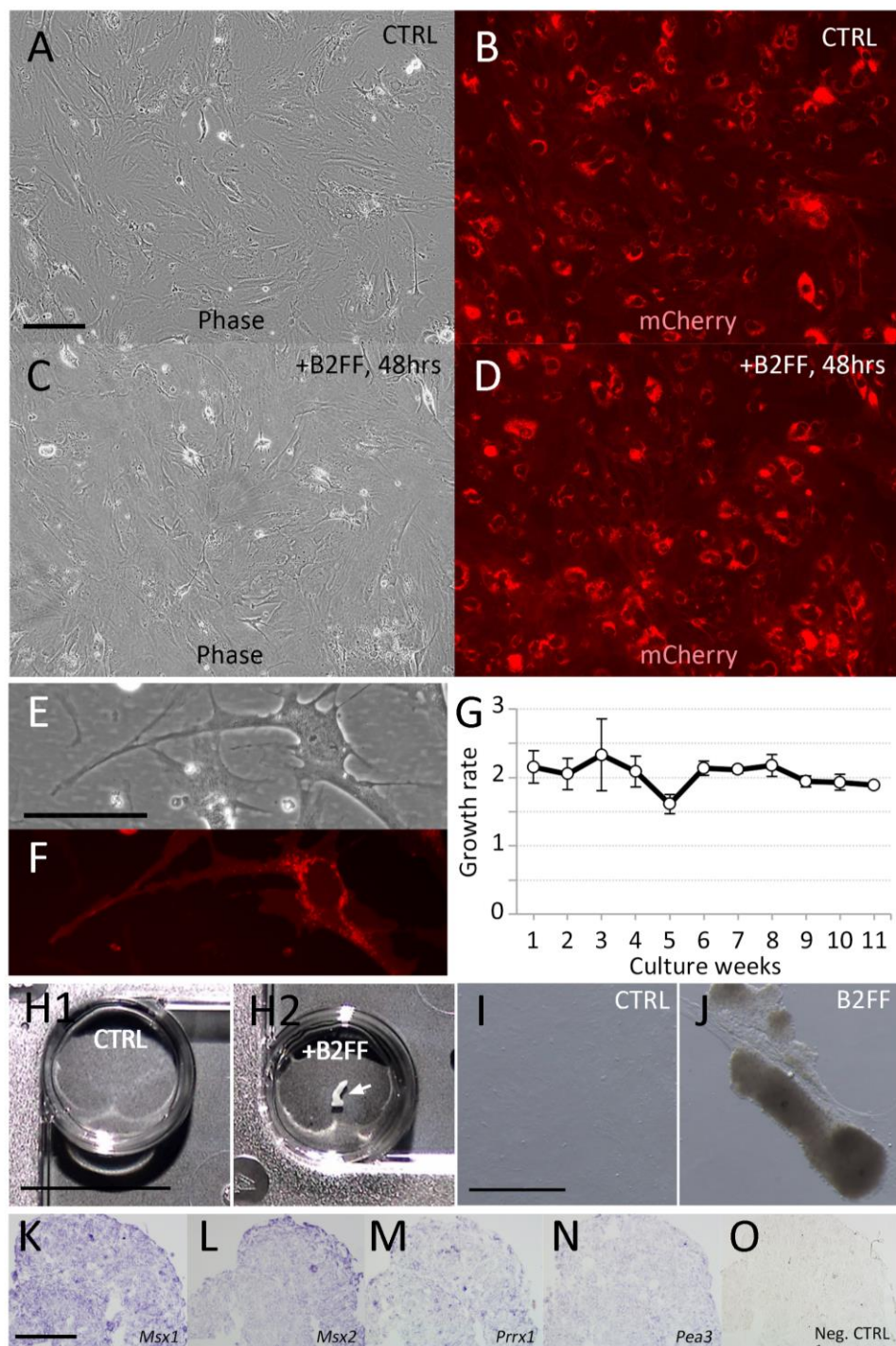
373 ***Competing interests:***

374 The authors have no conflicts of interest directly relevant to the content of this article.

375

376 *Figures and Figure legends*

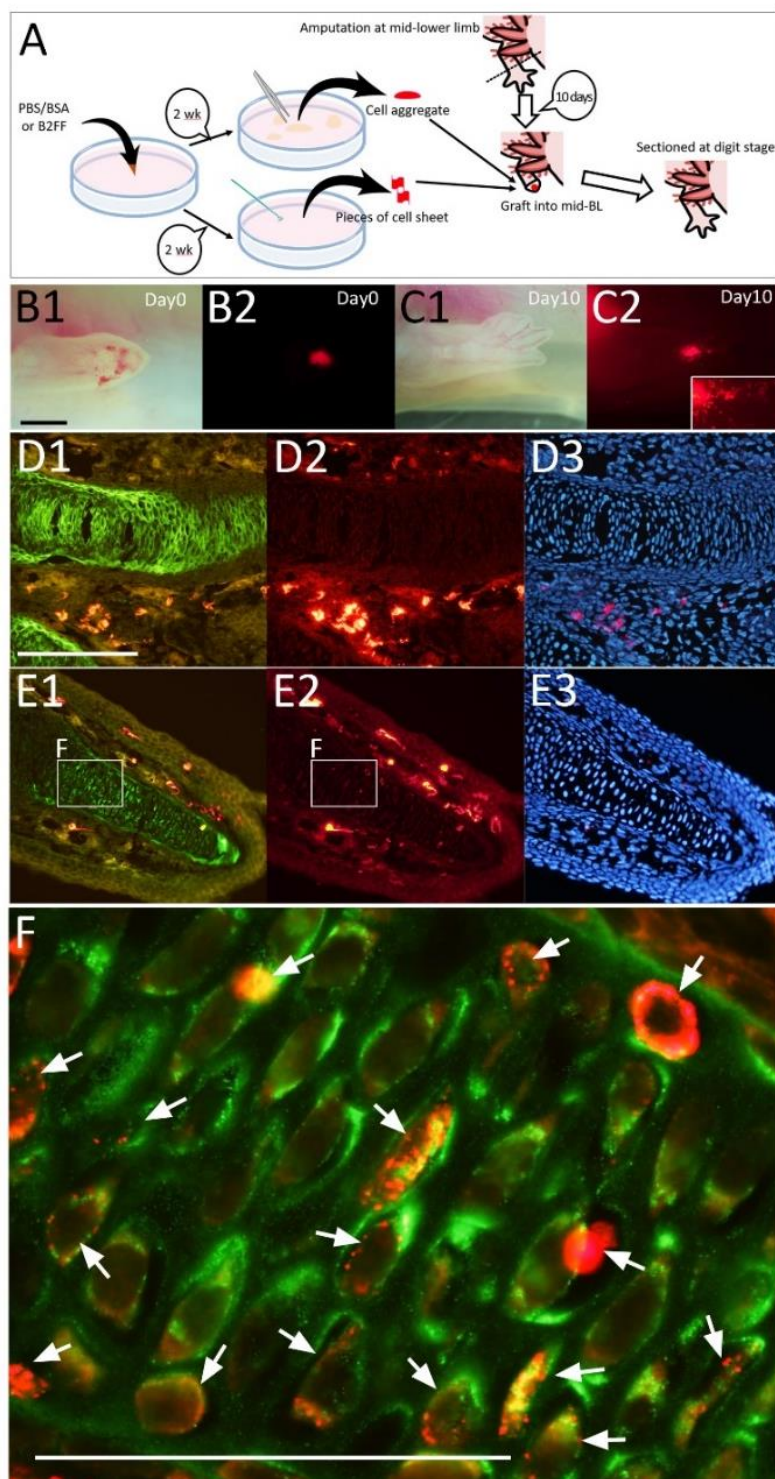
377 **Figure 1**





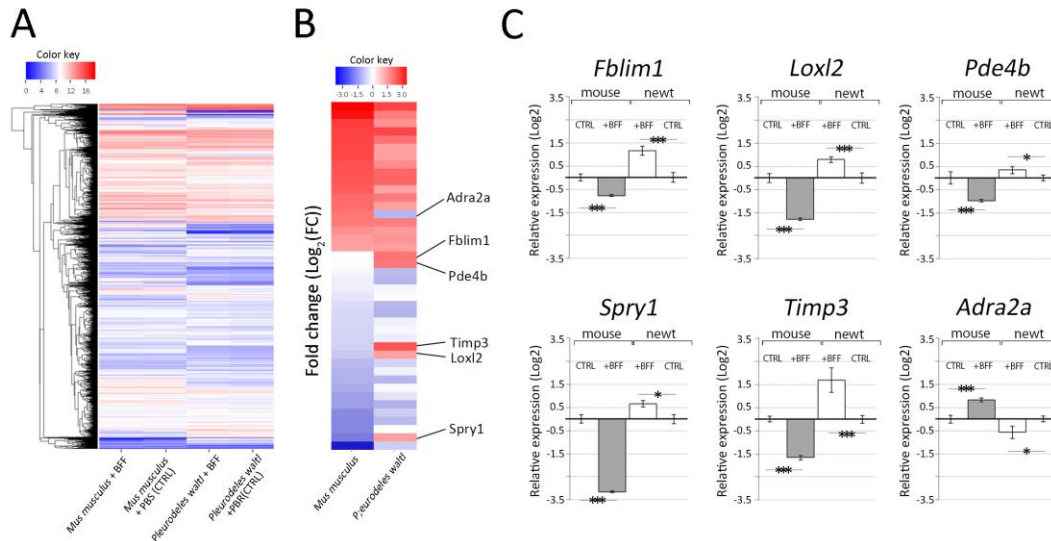
378 Cultured newt cells and B2FF application. (A, B) Newt cells in the control medium (no B2FF).  
379 (C, D) Newt cells 48h hours after the B2FF application. (A, C) Bright-field view. (B, D) Darkfield view.  
380 Scale bar in A = 500  $\mu\text{m}$ . (E, F) Higher magnification view of the newt cells in the control condition.  
381 Scale bar in E = 100  $\mu\text{m}$ . (G) The growth rate of the cultured newt cells in the control condition. (H1)  
382 Newt cells were kept for 2 weeks in the control condition. No cell aggregates could be observed. (H2)  
383 Newt cells were kept for 2 weeks in the B2FF-contained condition. Scale bar in H1 = 500  $\mu\text{m}$ . A large  
384 cell aggregate could be seen (arrow). (I, J) The bright-field images of the cells in the control (I) and the  
385 B2FF-contained (J) condition. Scale bar in I = 200  $\mu\text{m}$ . (K–O) Gene expression pattern of the aggregate  
386 formed in the B2FF condition was investigated by *in situ* hybridization. (O) the negative control (no  
387 probes). Scale bar in K = 300  $\mu\text{m}$ .

388 **Figure 2**



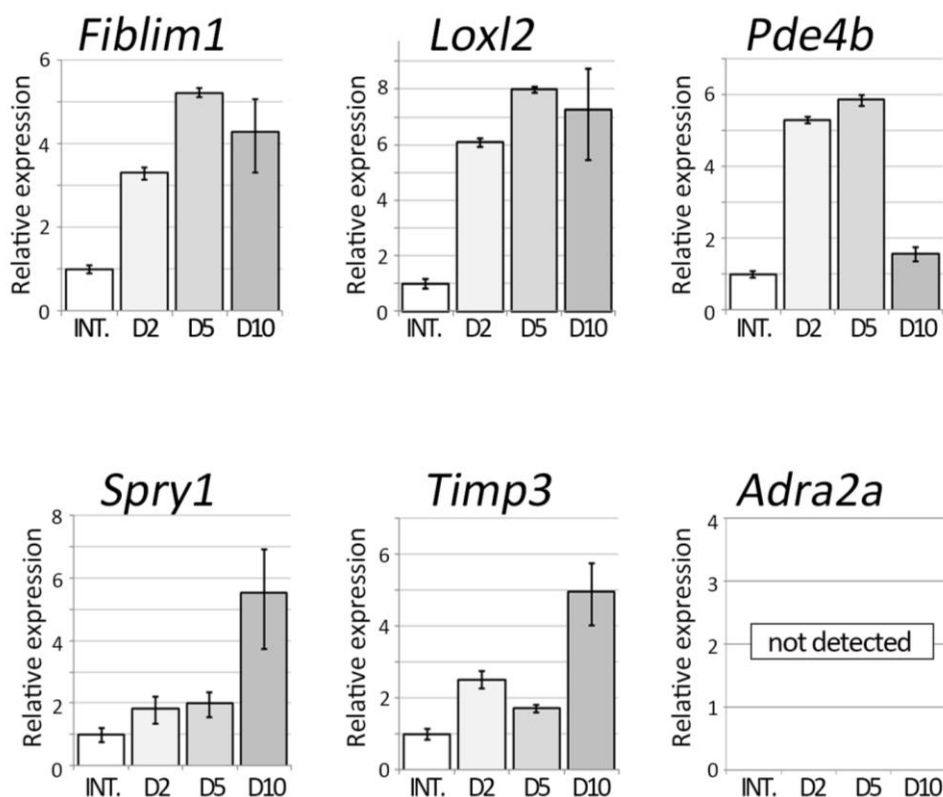
389           The cultured newt cells were grafted into regenerating axolotl limb blastema. (A) The  
390 schematic diagram of the experiment. (B) Just after the grafting. Scale bar in B1 = 1 mm. (C) 10 days  
391 after the grafting. Newt cells (red) were spread out in the regenerate (insert). (D–F) The distribution of  
392 the newt cells was investigated on the section. Immunofluorescent analysis for Col2a (green; D1 and E1)  
393 and mCherry (red; D2 and E2) was performed. Nuclei were visualized by Hoechst33342 (blue; D3 and  
394 E3). (F) the merged image of the boxed region in E1 and E2. The red signals were observable within the  
395 Col2a+ region. The scales bar in D1 and F are 300 and 100  $\mu$ m, respectively.

396 **Figure 3**



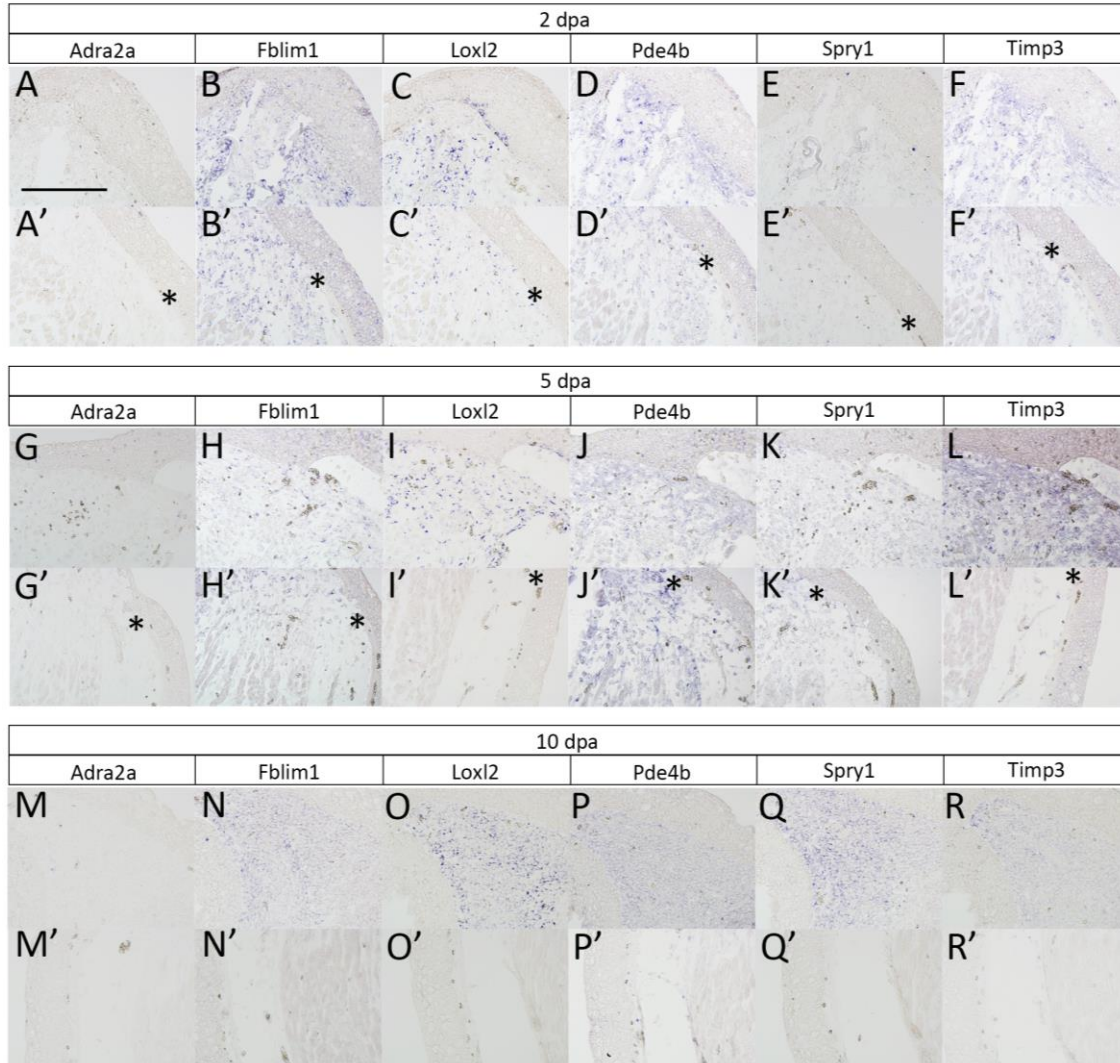
397 Selection of genes responding to B2FF in cell culture. (A) Z-score obtained via CAGE-seq is  
 398 visualized as the heatmap. The samples are mouse dermal fibroblasts with B2FF application, mouse  
 399 dermal fibroblasts without B2FF application (CTRL), newt dermal fibroblasts with B2FF application,  
 400 and newt dermal fibroblasts without B2FF application (CTRL) from the left. (B) the heatmap of the  
 401 selected genes, which were up/down-regulated by B2FF application. (C) the gene expression pattern was  
 402 confirmed by the quantitative RT-PCR. Genes, which were oppositely responded to B2FF in mouse and  
 403 newt cells, were selected and confirmed. \*p<0.05. \*\*\*p<0.01.

404 **Figure 4**



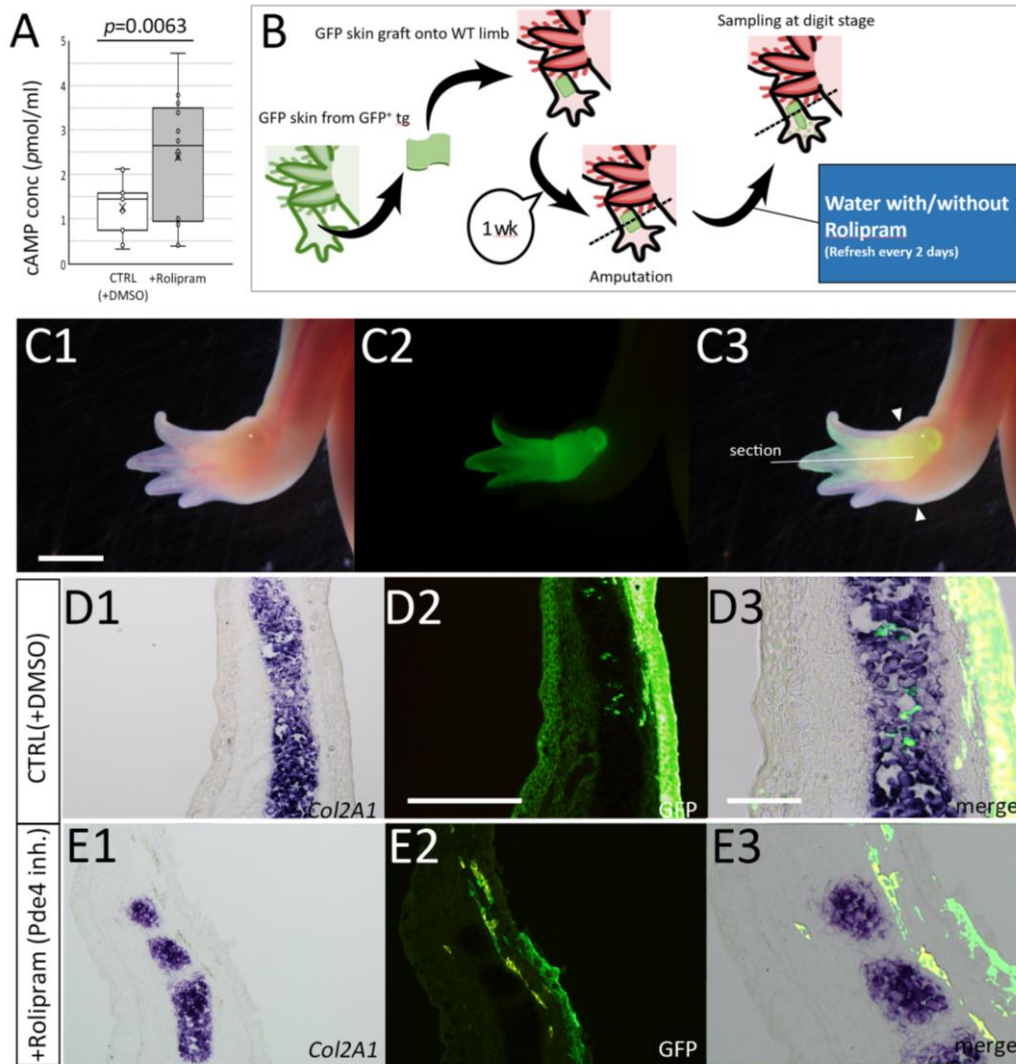
405 Gene expression patterns of the selected genes. The genes selected from the comparative  
406 analysis between the mouse and newt cells were investigated in axolotl blastemas. The quantitative  
407 RT-PCR to the samples, which were prepared from blastemas at different time points, was performed.  
408 INT. = intact limbs. D2 = 2 days after limb amputation.

409 **Figure 5**



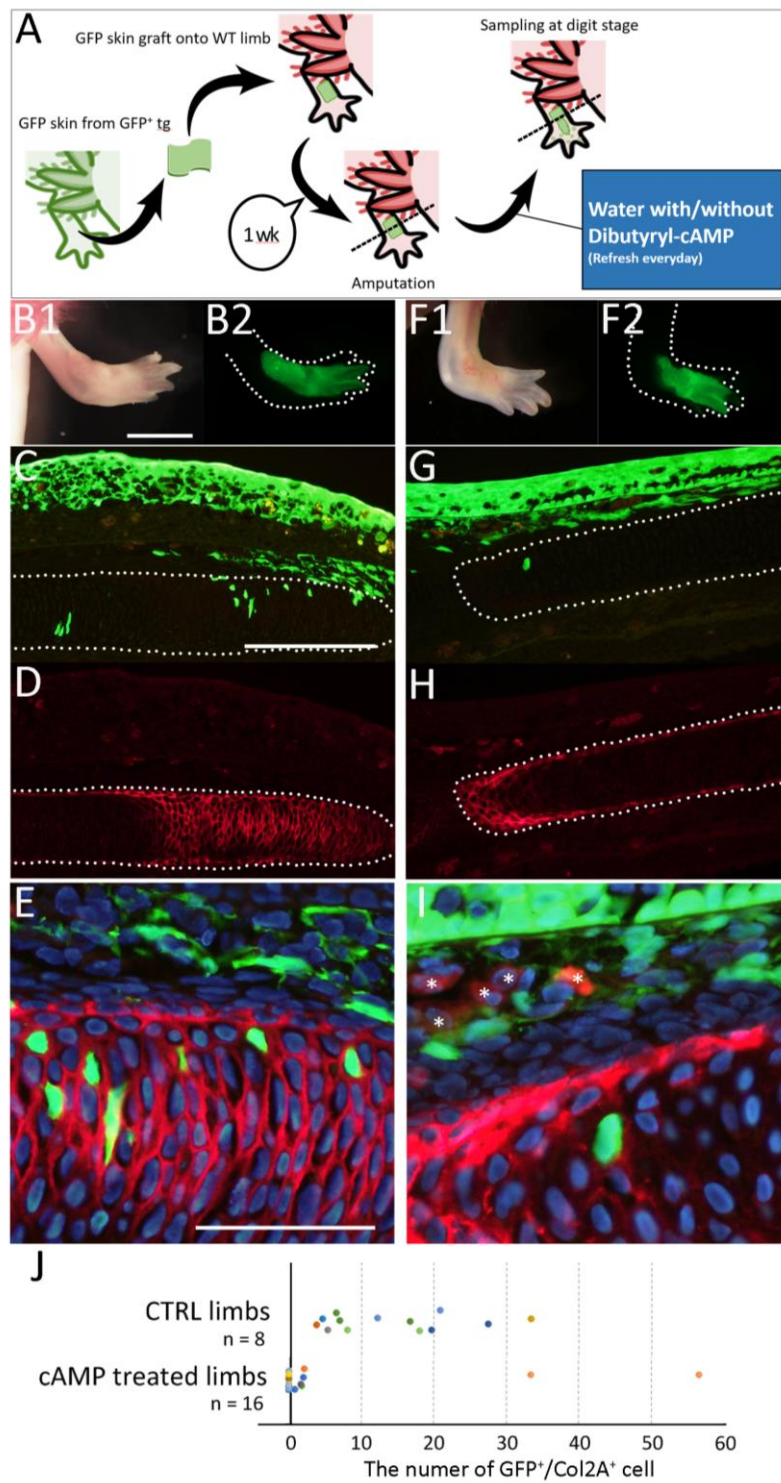
410 Gene expression patterns revealed by *in situ* hybridization. The blastema samples were  
 411 prepared at 2 dpa (A–F), 5 dpa (G–L), and 10 dpa (M–R). (A, G, M) expression pattern of *Adra2a*. (B, H,  
 412 N) expression pattern of *Fblim1*. (C, I, O) expression pattern of *Loxl2*. (D, J, P) expression pattern of  
 413 *Pde4b*. (E, K, Q) expression pattern of *Spry1*. (F, L, R) expression pattern of *Timp3*. The upper panels  
 414 (A–R) show the distal region of the amputated limbs. The lower panels (A'–R') show the proximal or the  
 415 approximate border of the amputation plane. The asterisks indicate the disconnection of the dermal  
 416 collagen layer, suggesting the amputation plane. Scale bar in A = 400  $\mu$ m.

417 **Figure 6**



418 Impaired transformation of dermal fibroblasts into cartilage cells by inhibition of Pde4b  
419 function by Rolipram. (A) Cyclic AMP concentration in limb tissues was measured by ELISA. (B) The  
420 schematic diagram of the experiment. (C) Rolipram treated limb in the bright-field view (C1), the dark  
421 field view (C2), and the merged image (C3). Scale bar in C1 = 3 mm. (D, E) Distribution of the GFP<sup>+</sup>  
422 cells in the regenerated limbs in the control (D) and the Rolipram treated animal (E). Col2a1 expression  
423 was visualized I by *in situ* hybridization (D1, E1) and GFP signals were detected by  
424 immunofluorescence (D2, E2) on the identical sections. D3 and E3 were the highly magnified and  
425 merged images. The scale bar in D2 and D3 are 300  $\mu$ m and 100  $\mu$ m, respectively.

426 **Figure 7**

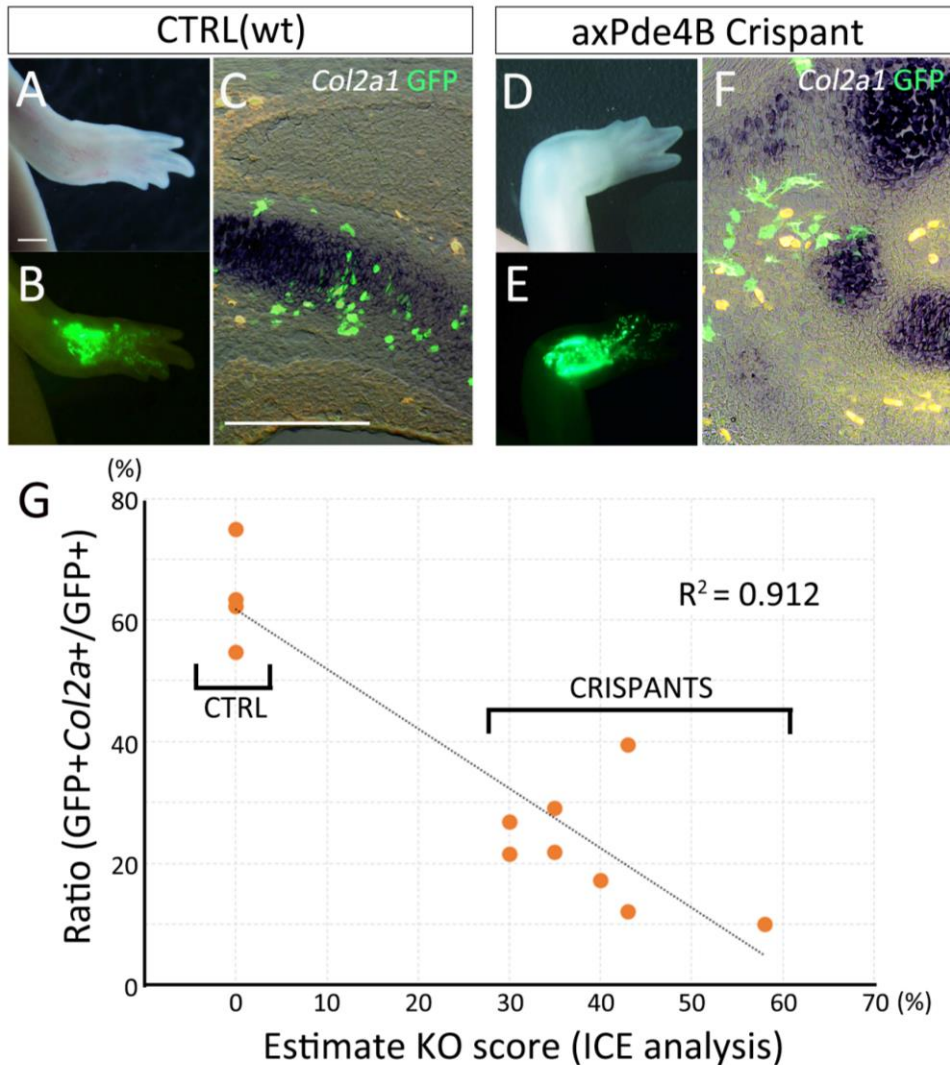




427                    Distribution of GFP<sup>+</sup> cells in the dibutyryl-cAMP treated animal. (A) the schematic diagram  
428 of the experiment. The GFP-skin grafted limb of the control animal (B–E) and the dibutyryl-cAMP  
429 treated animal (F–I). (B, F) The GFP-grafted limb just before sampling. (C–E, G–I) The distribution of  
430 the GFP<sup>+</sup> cells and Col2a expression were visualized by immunofluorescence. (E, I) the merged and  
431 higher magnified image of C and D. The asterisks in I indicate the red blood cells. The dotted lines  
432 indicate the border of the cartilage. (J) The plot of the number of GFP<sup>+</sup>Col2a<sup>+</sup> cells. The scale bars in B1,  
433 C, and E are 3 mm, 300  $\mu$ m, and 100  $\mu$ m, respectively.



444 **Figure 9**



445 Transdifferentiation from the dermis to cartilage in the mosaic Pde4b crispants. (A–C) the  
446 control animals (wt: wild-type). (D–E) The mosaic Pde4b crispants. (A, D) limb morphology. (B, E)  
447 The distribution of the GFP<sup>+</sup> cells. GFP plasmids were electroporated in the dermal region prior to  
448 amputation. (C, F) the merged images of the *Col2a1*, GFP, and the bright field view. *Col2a1* and GFP  
449 were visualized by *in situ* hybridization and immunofluorescence, respectively. The scale bars in A and  
450 C are 1 mm and 300  $\mu$ m, respectively. (G) the plot of the GFP+*Col2a1*+ / GFP+ ratio along with the KO  
451 score calculated by ICE analysis.

452 ***Materials and methods***

453 ***Animals and Cell culture***

454 Axolotls (*Ambystoma mexicanum*) with a nose-to-tail length of 4–8 cm were used. Small  
455 axolotls (3–4 cm) were used for chemical treatment. The GFP axolotls were from the Ambystoma  
456 Genetic Stock Center (AGSC, Univ. of Kentucky). The axolotls were housed in aerated water at 22 °C.  
457 Photoshop CS5 software (Adobe, San Jose, CA, US). Newts (*Pleurodeles waltl*) were obtained from  
458 Hiroshima University (Amphibian research center)<sup>30</sup>. All animal experiments were conducted following  
459 the guidelines of Okayama University.

460 The cells from a TgSceI (CAG::TVA-mCherry-p2A-Cas9) were isolated to obtain mCherry  
461 positive cells. Mouse cells were from the skin of C3H newborn mice (1 day old). Skin fibroblasts were  
462 isolated as follows. The limb skin was removed from a mCherry<sup>+</sup> animal by forceps and micro scissors.  
463 The skin was minced well and incubated in 0.5% collagenase solution (0.5% collagenase (Wako-Fuji  
464 film, Osaka, Japan) in 70% phosphate-buffered saline (PBS)) for 6 hours. Then, the equal amount of  
465 trypsin solution (0.5% Trypsin (Wako-Fuji film, Osaka, Japan) in PBS) was added and incubated for 30  
466 minutes. The solution was filtered by 45 µm mesh and enzymatic activity were neutralized by adding the  
467 culture medium (10% FBS, 40% Glutamax DMEM (ThermoFisher, MA, USA), 50% water, 300 µg/ml  
468 Gentamycin (Nakarai tesque, Kyoto, Japan), and 10 mM HEPES, pH 7.5). A couple of centrifugation  
469 was taken for wash, and then the cells were cultured on the plate. FGF2 (#3139), FGF8 (#423-F8), and  
470 BMP2 (#355-BM) (R&D Systems, MN, USA) were used and added to the medium at 0.1ug/ml  
471 concentration. Cell count for calculating the growth rate was performed by Countess II (Thermo Fisher).

472

473 ***CAGE-seq and RT-PCR***

474 CAGE-seq was performed by DNAFORM (Kanagawa, Japan). Total RNA was extracted from the  
475 cells, which were treated with PBS or B2FF for 48 hours. The samples were sent to DNAFORM  
476 (Kanagawa, Japan) in order to perform CAGE-seq. High-quality total RNA was prepared by Trizol  
477 (Invitrogen). Mapping of CAGE-tag sequences to the transcriptome assembly of *Pleurodeles waltl*  
478 (Trinity\_Pwal\_v2.fasta.gz, from iNewt website) was performed by Bowtie2. The read count was through  
479 the program featureCounts. The differential analysis was using DESeq2. Heatmap was described by  
480 Python. The quantitative RT-PCR was performed using primers listed in the supplemental Table 1. The  
481 RNA samples were prepared from 2 independent samples. The quantitative RT-PCR analysis was  
482 performed by StepOne™ (ThermoFisher) and KAPA DNA polymerase (#KK4600, NIPPON genetics,  
483 Tokyo, Japan).

484

485 ***Pde4b* knockout by CRISPR/Cas9 and ICE analysis**

486 The animals, in which the *Pde4b* gene was heterogeneously edited, were generated as  
487 described<sup>30</sup>. The two guide RNAs were prepared as follows; gPde4b ver1:  
488 GGAGGAGCTGGACTGGTGCC, gPde4b ver2: GTCCGTGTGCTTGTTCAG. The guide RNA and  
489 sgRNA were purified using a CUGA gRNA synthesis kit. The synthesized gRNA was incubated with  
490 Cas9 proteins (IDT) for 30 minutes at room temperature before injection.

491 Gene knockout score was calculated by ICE analysis (<https://ice.synthego.com/#/>). The axolotl  
492 genome for the ICE analysis was extracted from the limb skin. The small piece of the forelimb skin was  
493 removed from an upper arm and the genome was purified using the QIAGEN genome extraction kit  
494 (#69506). The standard Sanger sequence was performed to the amplified genomic PCR fragment using  
495 the following primers; for: ATGATGAAGGAGCACTGCCCCACC; rev:  
496 CTTGTTTCGATGCCATCTCGCTGACG.

497  
498 ***Electroporation***

499 Electroporation was performed as previously described<sup>9</sup>. Briefly, pCS2-AcGFP plasmids (1  
500 µg/µl) were injected underneath of the skin. The electrodes were placed as nipping the injection site.  
501 The electroporation was performed under the following condition; 20V, 50ms pulse, 950 ms interval, and  
502 20 times). The electroporated animals were kept for 3 days and checked the fluorescent signals were  
503 under a microscope.

504  
505  
506 ***Cell Grafting***

507 Cultured newt cells were grafted into axolotl limbs. Cell aggregates or sheets were from  
508 14-days cultured wells. Aggregated were formed in the B2FF medium. The aggregates were easily  
509 removed from the plastic dish by forceps. Regarding to the wells filled by the regular medium, no  
510 aggregates were formed. Cell sheets were isolated by a cell scraper. The isolated cell aggregates or  
511 sheets were transferred into an axolotl blastema that was grown for 10 days. The grafted limbs were  
512 raised until digits were formed.

513  
514 ***Inhibitor treatment***

515 Rolipram (Tokyo Chemical Industry, Tokyo, Japan) was dissolved in dimethyl sulfoxide  
516 (DMSO; Nacalai Tesque, Kyoto, Japan), to prepare a 130 mM stock solution. For inhibitor treatment, we

517 kept the animals in the presence of Rolipram (130  $\mu$ M) or DMSO, in water. The water was changed  
518 every day until the samples were fixed.

519

### 520 ***Sectioning, histological staining, and in situ hybridization***

521 Tissue samples were fixed with 4% paraformaldehyde/PBS for 1 day at room temperature, and  
522 the fixed tissues were treated in 30% sucrose/PBS at 4 °C for 1 day. Then, the samples were embedded  
523 in the O.C.T compound (Sakura Finetech, Tokyo, Japan). Frozen sections of 14- $\mu$ m thickness were  
524 prepared using a Leica CM1850 cryostat (Leica Microsystems, Wetzlar, Germany). The sections were  
525 dried under an air dryer. For histological observation, standard trichrome staining was performed using  
526 the Trichrome Stain (Masson) Kit (Sigma-Aldrich, St. Louis, MO, USA). The stained sections were  
527 mounted using Softmount (Wako Pure Chemical Industries, Osaka, Japan). Immunofluorescence on the  
528 sections was carried out according to previously reported methods (Satoh et al., 2007). Anti-GFP (#594,  
529 MBL, Tokyo, Japan, 1:500), anti-Col2 antibody (II-II6B3, DSHB, IW, USA, 1:200), anti-tenascin C  
530 antibody (MT1, DSHB), anti-rabbit IgG Alexa 488 (ab150077, 1:500) and anti-mouse IgG Alexa 594  
531 (A21203, 1:500; Invitrogen, CA, USA) were used for the immunofluorescence procedure. For the Col2  
532 immunofluorescence, antigen retrieval was necessary (Proteinase K (5 $\mu$ g/ml) for 30 minutes at room  
533 temperature). Images were captured using an Olympus BX51 system (Olympus Life Science, Tokyo,  
534 Japan). Nuclei were visualized by Hoechst 33342 (Wako-Fuji film, #346-07951). RNA probes and *in*  
535 *situ* hybridization procedures have previously been described (Makanae et al., 2014). Cell counts on the  
536 images were performed by Photoshop CS6 software (Adobe).

537

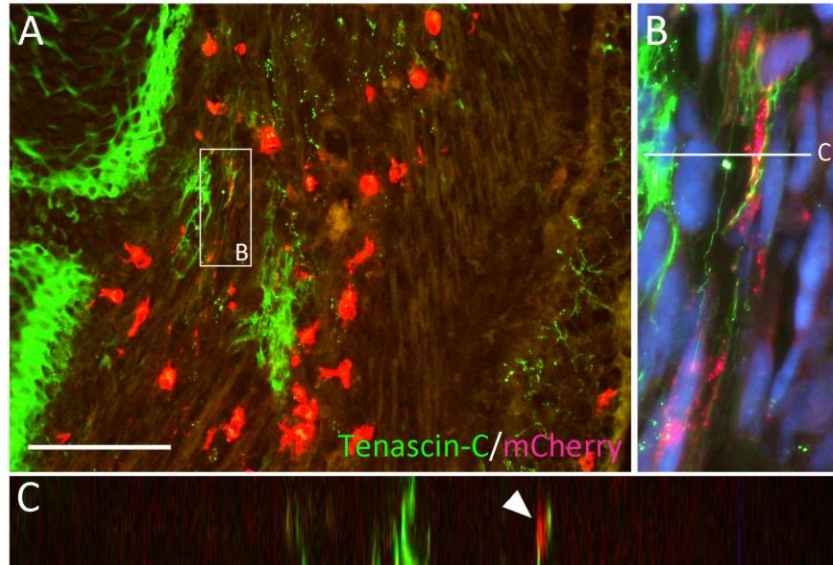
### 538 ***ELISA***

539 ELISA was performed using Cayman cyclic AMP ELISA kit (#581001, Cayman Chemical, MI,  
540 USA). Samples were prepared from the Rolipram treated animals and control (DMSO treated) animals.  
541 Limbs were isolated from the animals and used for the analysis. We set the wavelength at 410 nm, and  
542 the absorbance was measured by the microplate reader (CORONA, MTP-880lab). Six limbs of each  
543 treatment were independently measured.

544

545 **Supplemental Figure legends**

546 **Supplemental Figure 1**



547 The distribution of the mCherry+ newt cells in the axolotl regenerated limb and Tenascin-C  
 548 expression. (A) The signals of mCherry and Tenascin-C were visualized by immunofluorescence. The  
 549 scale bar in A is 200  $\mu\text{m}$ . (B) The higher magnification view of the boxed region in A. The blue color  
 550 indicates the nuclei. (C) The side view of the region is indicated by the line in B. The Tenascin-C signal  
 551 is located at the side of the mCherry+ cytoplasm (arrowhead).

552 **Supplemental Figure 2**



553 The comparison of the amino acid sequences of PDE4B. The amino acid sequence of PDE4B  
 554 shown in the figure indicates the nearby region where Rolipram binds. The amino acids surrounded by  
 555 green lines indicate the residue to which Rolipram forms a hydrogen bond. The amino acid sequence  
 556 boxed with the orange line indicates the non-ligand residue involved in hydrophobic contact(s).

557 **References**

- 558 1. Muneoka K, Bryant SV. Evidence that patterning mechanisms in developing and regenerating  
559 limbs are the same. *Nature* **298**, 369-371 (1982).  
560
- 561 2. Gerber T, *et al.* Single-cell analysis uncovers convergence of cell identities during axolotl limb  
562 regeneration. *Science* **362**, eaaq0681 (2018).  
563
- 564 3. Nye HL, Cameron JA, Chernoff EA, Stocum DL. Regeneration of the urodele limb: a review.  
565 *Developmental dynamics : an official publication of the American Association of Anatomists*  
566 **226**, 280-294 (2003).  
567
- 568 4. Satoh A, Mitogawa K, Makanae A. Regeneration inducers in limb regeneration. *Development,*  
569 *Growth & Differentiation* **57**, 421-429 (2015).  
570
- 571 5. Tsonis PA. *Limb regeneration*. Cambridge University Press (1996).  
572
- 573 6. Farkas JE, Freitas PD, Bryant DM, Whited JL, Monaghan JR. Neuregulin-1 signaling is  
574 essential for nerve-dependent axolotl limb regeneration. *Development (Cambridge, England)*  
575 **143**, 2724-2731 (2016).  
576
- 577 7. Kumar A, Godwin JW, Gates PB, Garza-Garcia AA, Brookes JP. Molecular basis for the nerve  
578 dependence of limb regeneration in an adult vertebrate. *Science (New York, NY)* **318**, 772-777  
579 (2007).  
580
- 581 8. Makanae A, Mitogawa K, Satoh A. Co-operative Bmp- and Fgf-signaling inputs convert skin  
582 wound healing to limb formation in urodele amphibians. *Developmental biology* **396**, 57-66  
583 (2014).  
584
- 585 9. Satoh A, Makanae A, Nishimoto Y, Mitogawa K. FGF and BMP derived from dorsal root  
586 ganglia regulate blastema induction in limb regeneration in *Ambystoma mexicanum*.  
587 *Developmental biology* **417**, 114-125 (2016).  
588
- 589 10. Muneoka K, Fox WF, Bryant SV. Cellular contribution from dermis and cartilage to the



- 590 regenerating limb blastema in axolotls. *Developmental biology* **116**, 256-260 (1986).  
591
- 592 11. Gardiner DM, Muneoka K, Bryant SV. The migration of dermal cells during blastema formation  
593 in axolotls. *Developmental biology* **118**, 488-493 (1986).  
594
- 595 12. Hirata A, Makanae A, Satoh A. Accessory limb induction on flank region and its muscle  
596 regulation in axolotl. *Developmental dynamics : an official publication of the American*  
597 *Association of Anatomists* **242**, 932-940 (2013).  
598
- 599 13. Kragl M, *et al.* Cells keep a memory of their tissue origin during axolotl limb regeneration.  
600 *Nature* **460**, 60-65 (2009).  
601
- 602 14. Gilbert SF, Barresi MJF. *Developmental biology* (2018).  
603
- 604 15. Cohen N. Chronic skin graft rejection in the Urodela. II. A comparative study of xenograft  
605 rejection. *Transplantation* **7**, 332-346 (1969).  
606
- 607 16. Onda H, Goldhamer DJ, Tassava RA. An extracellular matrix molecule of newt and axolotl  
608 regenerating limb blastemas and embryonic limb buds: immunological relationship of MT1  
609 antigen with tenascin. *Development (Cambridge, England)* **108**, 657-668 (1990).  
610
- 611 17. Makanae A, Hirata A, Honjo Y, Mitogawa K, Satoh A. Nerve independent limb induction in  
612 axolotls. *Developmental biology* **381**, 213-226 (2013).  
613
- 614 18. Satoh A, Gardiner DM, Bryant SV, Endo T. Nerve-induced ectopic limb blastemas in the  
615 Axolotl are equivalent to amputation-induced blastemas. *Developmental biology* **312**, 231-244  
616 (2007).  
617
- 618 19. Fertig BA, Baillie GS. PDE4-Mediated cAMP Signalling. *J Cardiovasc Dev Dis* **5**, 8 (2018).  
619
- 620 20. Schwede F, Maronde E, Genieser H, Jastorff B. Cyclic nucleotide analogs as biochemical tools  
621 and prospective drugs. *Pharmacology & therapeutics* **87**, 199-226 (2000).  
622

- 623 21. de Both NJ. Transplantation immunity in the axolotl (*Ambystoma mexicanum*) studied by  
624 blastemal grafts. *Journal of Experimental Zoology* **173**, 147-158 (1970).  
625
- 626 22. Cohen N. Amphibian Transplantation Reactions: A Review. *American Zoologist* **11**, 193-205  
627 (2015).  
628
- 629 23. Satoh A, Mitogawa K, Makanae A. Nerve roles in blastema induction and pattern formation in  
630 limb regeneration. *The International journal of developmental biology* **62**, 605-612 (2018).  
631
- 632 24. Denis J-F, Sader F, Ferretti P, Roy S. Culture and Transfection of Axolotl Cells. In: *Salamanders*  
633 *in Regeneration Research: Methods and Protocols* (eds Kumar A, Simon A). Springer New  
634 York (2015).  
635
- 636 25. Makanae A, Satoh A. Early Regulation of Axolotl Limb Regeneration. *The Anatomical Record*  
637 **295**, 1566-1574 (2012).  
638
- 639 26. Johnson GL, Masias EJ, Lehoczy JA. Cellular Heterogeneity and Lineage Restriction during  
640 Mouse Digit Tip Regeneration at Single-Cell Resolution. *Developmental Cell* **52**, 525-540.e525  
641 (2020).  
642
- 643 27. Meinkoth JL, *et al.* Signal transduction through the cAMP-dependent protein kinase. *Molecular*  
644 *and Cellular Biochemistry* **127**, 179-186 (1993).  
645
- 646 28. Sicard RE. The effects of hypophysectomy upon the endogenous levels of cyclic AMP during  
647 forelimb regeneration of adult newts (*Notophthalmus viridescens*). *Wilhelm Roux's archives of*  
648 *developmental biology* **177**, 159-162 (1975).  
649
- 650 29. Wallace H. Vertebrate limb regeneration.) (1981).  
651
- 652 30. Hayashi T, *et al.* Molecular genetic system for regenerative studies using newts. *Development,*  
653 *Growth & Differentiation* **55**, 229-236 (2013).  
654  
655

